Permeability of electrospun fiber mats under pressure driven flow

Citation: Choong, Looh Tchuin (Simon), Zafarullah Khan, and Gregory C. Rutledge. "Permeability of Electrospun Fiber Mats Under Hydraulic Flow." Journal of Membrane Science 451 (February 2014): 111–116.

As Published: http://dx.doi.org/10.1016/j.memsci.2013.09.051

Publisher: Elsevier

Persistent URL: http://hdl.handle.net/1721.1/101388

Version: Author's final manuscript: final author's manuscript post peer review, without publisher's formatting or copy editing

Permeability of Electrospun Fiber Mats Under Pressure Driven Flow

Looh Tchuin (Simon) Choong[1], Zafarullah Khan[2], Gregory C. Rutledge[1*]

[1]Department of Chemical Engineering, Massachusetts Institute of Technology

[2]King Fahd University of Petroleum and Minerals, Dhahran, Saudi Arabia

[*]Corresponding author. Tel.: +1 617 253 0171; fax: +1 617 258 5766.

E-mail address: rutledge@mit.edu (G. C. Rutledge).

Abstract

Hydraulic permeability of electrospun fiber mats under flow-induced compression has been modeled and verified experimentally. The permeation model accurately estimates the changes in solidity, and hence the permeability of the electrospun mats, over a range of pressure differentials. The model is based on Darcy's law applied to a compressible, porous medium, using Happel's equation for the permeability and Toll's equation for the compressibility of fiber mats. Hydraulic permeability of electrospun mats of bis-phenol A polysulfone (PSU) comprising fibers of different mean diameter, annealed at temperatures at and above the glass transition of the polymer, was measured for feed water pressures ranging from 5 kPa to 140 kPa. The electrospun mats are found to experience a decrease of more than 60% in permeability constant between 5 and 140 kPa due to the loss of porosity resulting from the flow-induced compression.

Keywords: Permeability, compression, nanofibers, electrospinning

1. Introduction

Electrospun fiber mats are promising for many filtration applications like coalescence filtration, depth filtration, etc., because of their high porosity (>0.9) and small inter-fiber distances (typically 0.1-10 μm), which provide high permeabilities and high separation efficiencies [1,2]. However, electrospun fiber mats are also highly compressible [22], hence their porosity decreases with increasing pressure. This compressibility of the mat can counter the benefits of high porosity in filtration applications. An understanding of

the extent of the reduction in permeance upon compression for electrospun fiber mats is vital for evaluating their performance relative to other, commercial filtration membranes under conditions relevant for filtration processes. A typical operating pressure for an ultrafiltration process is 10^5 Pa, and for reverse osmosis can be up to 10^7 Pa [3].

The studies of flow through compressible media are diverse. Biot [4,5] developed the theory of the consolidation of porous soil containing a viscous fluid; Mow, Lai and co-workers [6,7] studied the effects of compressive strain-dependence on the fluid permeability of articular cartilage. Zhu et al. [8] and Kataja et al. [9] modeled water permeation during wet pressing of paper. Jönsson and Jönsson [10,11] modeled filtration through compressible porous media as the gradual transformation of hydraulic pressure into mechanical stress on the porous solid. The main difference between the systems mentioned above is the structure of the porous network, which affects the expressions of permeability constant and compressibility. Here, we adopt the approach of Jönsson and Jönsson, combined with expressions for the permeability and compressibility of fibrous materials to describe the flux of water through electrospun mats.

The permeability of porous fibrous media has been studied extensively. Equations for permeability constants that account for the drag forces exerted on the liquid by the solid medium have been developed for flow through a 2-D array of cylinders that are aligned parallel [12,13] or perpendicular [12,13,14] to the direction of the flow, as well as through 3-D random arrays of cylinders [15]. Mao and Russell [16,17] included the effect of fiber orientation in both 2-D and 3-D arrays. Others have also studied the permeability numerically and developed the permeability equations empirically from experimental data [18,19,20]. Electrospun mats can be approximated as planar fibrous networks. From the review by Jackson and James [21], analytical permeability models for flow perpendicular to a 2-D array of cylinders developed by Happel [12] and by Spielman and Goren [15] fit the experimental data well in the solidity range ~0.05 to 0.3 (where solidity is defined as 1–porosity). Since Happel's equation is considerably simpler and does not involve implicit functions of permeability, Happel's model is chosen for this work.

The compressibility of electrospun mats can be described by a power-law equation that correlates the compressive stress (σ_m) applied to electrospun mats with the solidity (ϕ) of the mats:

$$\sigma_m = kE(\phi^n - \phi_0^n) \quad (1)$$

where k is an empirical constant that accounts for variations in the length, contour, and other characteristics of the fiber segments between load-bearing contacts; E is the Young's modulus of the fiber; ϕ and ϕ_0 are the solidity under compression and the initial solidity of the fibrous medium at zero stress, respectively; and n is the exponent, which depends on the nature of the fiber network. We have previously validated Eq. 1 experimentally for electrospun fiber mats [22], and studied the effect of thermal annealing on compressibility of electrospun mats. For details of the derivation of Eq. 1, the reader is referred to the original work of Toll [23].

2. Modeling of Permeation

In Jönsson's work [10], the total pressure (P_{tot}) associated with fluid flow through a porous medium system is the sum of the hydraulic pressure (P_h) that drives the fluid flow through the porous medium, and the mechanical stress (σ_m) that deforms the porous medium. The mechanical stress arises from the drag of fluid on the surface of the medium as the fluid flows. The drag also results in the drop of the hydraulic pressure in the direction of the flow [12]. The mechanical stress on the fiber mat increases in the flow direction because the force propagates via the fiber-fiber contacts [23]. Therefore, the last layer of the porous medium in the flow direction experiences the largest compression, as shown qualitatively in Figure 1. The P_{tot} is equal to the trans-membrane pressure drop, ΔP.

The flux of water (J) through an electrospun mat, which is a fibrous porous medium, can be described by Darcy's law:

$$J = -\frac{K}{\mu}\frac{dP_h}{dz} \quad (2)$$

where K is the permeability constant, μ is the dynamic viscosity of water, and dP_h/dz is the hydraulic pressure gradient through the thickness of the mat. The negative sign is due

to the convention used in this work, where z = 0 at the inlet of the mat. Since the sum of σ_m and P_h is constant ($\sigma_m = P_{tot} - P_h$), we can rewrite Eq.2 in term of σ_m.

$$J = \frac{K}{\mu}\frac{d\sigma_m}{dz} \tag{3}$$

The permeability constant for a highly porous fibrous medium has been derived analytically for flow around a cylinder by Happel [12].

$$K = \frac{D^2}{32\phi}\left(-ln\phi + \frac{\phi^2-1}{\phi^2+1}\right) \tag{4}$$

where D is the fiber diameter. Eq.1 was used to account for the compression of the electrospun mat.

Given the basis weight and pressure drop across the membrane, we make an initial guess for flux (J) and integrate eqs (5) and (6) from $\phi = \phi_0$ and σ_m=0 at z = 0 to σ_m=P_{tot}. From the profile thus obtained for $\phi(z)$, the error in basis weight can be determined, and the value for flux iterated until the correct basis weight is obtained.

$$\frac{dz}{d\sigma_m} = \frac{K}{J\mu} \tag{5}$$

$$\frac{d\phi}{d\sigma_m} = \frac{1}{nkE\phi^{n-1}} \tag{6}$$

During an experiment, the flux (J) and the trans-membrane pressure drop (ΔP) were measured, from which the permeance, defined as $J/\Delta P$, was computed and compared to that predicted by the model. To convert permeance to permeability, it is also necessary to know the mat thickness during flow; the mat thickness, and thus permeability K, was obtained by application of the model

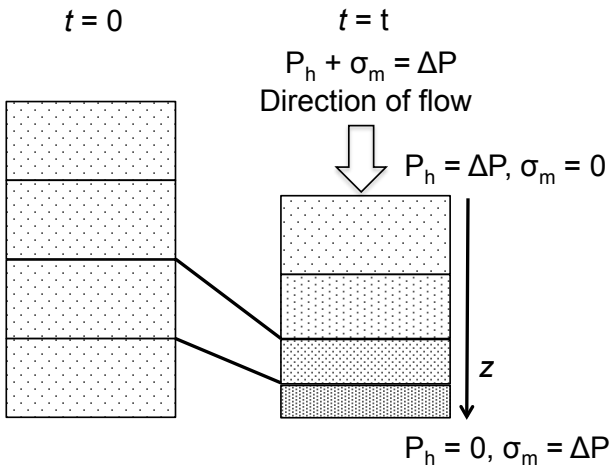

Figure 1. Schematic of deformation of an electrospun mat under pressure driven flow. The density of the dots represents qualitatively the degree of compaction [10].

3. Experimental

3.1 Materials. Bisphenol-A-polysulfone (PSU), purchased from Sigma Aldrich, is a glassy amorphous solid at room temperature, with a glass transition temperature of 188°C, as measured by Differential Scanning Calorimetry (DSC, TA Q100). N,N-dimethyl formamide (DMF) was obtained from Sigma-Aldrich and used as received, as solvent for preparing the PSU solutions for electrospinning. Formic acid (FA) was added to some solutions in small amounts to modify their electrical properties, to allow some control of fiber diameter. Cellulose acetate microfiltration (MF) membrane with a nominal pore size of 3μm and thickness of (167±2) μm (measured using Agilent UTM as described in section 3.5) was purchased from Millipore (SSWP02500) and used as received.

3.2 Fabrication. A vertically aligned, parallel plate setup was used for electrospinning, as described elsewhere [24]. The top plate was 15 cm in diameter and charged with a high voltage supply (Gamma High Voltage Research, ES40P) to a voltage in the range of 10-30 kV. The grounded bottom plate, which also served as the collector for the fiber mat, was a 15cm x15cm stainless steel platform. The tip-to-collector distance was varied from 25 to 35 cm by adjusting the height of the bottom plate. The polymeric solution was

loaded into a syringe attached by Teflon tubing to a stainless steel capillary (1.6 mm OD, 1.0 mm ID) that protruded 21 mm through the center of the top plate. A digitally controlled syringe pump (Harvard Apparatus, PHD 2000) was used to control the flow rate of the polymer solution in the range of 0.005-0.02mL/min.

3.3 Post-processing. The as-spun mats were annealed thermally in a furnace (Thermolyne Industrial Benchtop Furnace, FD1545M) to strengthen the electrospun mat, as previously reported [24]. The mats were held in plane during the annealing process by draping over a petri dish that is 10 cm in diameter. The PSU mats were annealed at temperatures between 190 and 210 °C, which are above the glass transition temperature (T_g=188° C) of PSU, for one hour.

3.4 Characterization. The average fiber diameter of the electrospun fiber mats was calculated from the measurement of 30 to 50 fibers in images taken with a scanning electron microscope (SEM, JEOL-JSM-6060). The initial solidity was calculated by

$$\phi_0 = \frac{\phi_{0.5N} t_{0.5N}}{t_0}, \qquad (7)$$

where $\phi_{0.5N}$ is the solidity calculated using a gravimetric method in which the mat thickness ($t_{0.5N}$) was measured using an adjustable measuring force digital micrometer (Mutitoyo, Model CLM 1.6"QM) with a contact force of 0.5N. The quantity t_0 is an estimate of the mat thickness based on the probe position of the Agilent T150 UTM at 20μN contact force (*c.f.* compression test, next section).

3.5 Compression test. An unconfined uniaxial compression test was carried out using the Agilent T150 UTM (Agilent Technologies, Chandler, AZ) with a load cell of 500 mN. The electrospun fiber mats tend to be metastably hydrophobic due to their texture and porosity. To improve wettability, the mats were plasma treated by a plasma cleaner (Harrick PDC-32G) for one minute at the low power setting, and then soaked by water right after the treatment. Moreover, the compression test is performed on a wetted sample because the flow-induced compression of the mats occurs in a water-filled state. Five 1 mm diameter discs were cut from each of the wet, annealed mats using a micro punch with a 1.0mm tip (TedPella, Harris Micro Punch). Excess surface water was removed by

using KimWipes. Each of the discs was subjected to five cycles of loading and unloading in compression, with a maximum load of 50mN in each cycle. The first four cycles were used to condition the mats, as described previously [22], and the unloading curve of the fifth cycle was used for analysis. The compression was carried out at a loading strain rate of $0.01s^{-1}$ according to the ASTM D575 procedure [25] with an unloading rate of 1mN/s. The surface of the compression platens was lubricated with Teflon spray. The applied load (F) on the specimen and the corresponding change in thickness (Δt) of the specimen were recorded.

The planar surface area (A_{comp} = $0.785mm^2$, assumed to be constant), initial thickness (t_0) and initial solidity (ϕ_0) of the mat were used to convert the raw data from the UTM into mechanical stress ($\sigma_m = F/A_{comp}$), engineering strain ($e=\Delta t/t_0$) and solidity.

$$\phi = \frac{\phi_0 t_0}{t_0 - \Delta t} \tag{8}$$

t_0 was measured by the UTM with a contact force of 20μN as described above. Eq. 1 was fitted to the post-processed data of the unloading segment of the fifth cycle in log-log form using unconstrained nonlinear optimization with trust-region algorithm (`fminunc` in MATLAB v2011b), and the corresponding kE and n values were obtained. For further details, the reader is referred to the work of Choong et al. [22] on electrospun PSU mats evaluated in the dry state.

3.6 Permeance Measurement. The permeation test was carried out using a 25mm diameter, polypropylene in-line filter holder (Sterlitech, PP25) as the dead-end filtration cell. The electrospun mats were plasma treated at low power setting for one minute, and then soaked in deionized (DI) water to ensure that the mats were fully wetted. The average of the permeance was calculated from three replicates. The permeance of water was measured for pressures ranging from 5 kPa to 140 kPa. The pressure was controlled by a pressurized air supply applied to the water on the feed side of the mat. Each mat was conditioned by flowing water through at 140kPa for one minute before the permeation test. A permeation test consisted of measuring the permeance at successively higher pressures (from 5kPa to 140kPa) on the upstream side of the mat.

3.7 Permeance Modeling. The differential equations (Eq. 5 and 6) were solved numerically using backward differentiation formulae with orders 1 to 5 (`ode15s` in MATLAB v2011b) for solving stiff sets of equations. The inputs to the model were fiber diameter, mass and area of the membrane, thickness (t_0), and the values for n and kE obtained from compression testing; the outputs were the permeance and the profiles for pressure and solidity through the thickness of the mat. Since the value of kE value obtained from the compression test was judged to be imprecise [22], the kE value was then used as an adjustable parameter to fit the experimental permeance curve using a nonlinear equations solver with Levenberg-Marquardt algorithm (`fsolve` in MATLAB v2011b).

4. Results and Discussions

4.1 Morphology. As-spun PSU mats with fiber diameter of (0.8 ± 0.4) μm and (0.4 ± 0.1) μm were successfully electrospun, as shown in Figure 2. The average fiber diameter of the PSU mat annealed at 210°C was slightly larger than that of the as-spun mat, as shown in Table 1. This could be due to fibers welded together not only at the fiber-fiber contacts, but also along the fiber itself, at 210°C. PSU mats with smaller fiber diameter (0.4 μm) have narrower fiber diameter distributions than those of PSU mats with larger fiber diameter (0.8 μm). The initial solidity (ϕ_0), i.e. before any deformation, is independent of the annealing temperature of PSU mats but smaller for PSU with smaller fiber diameter.

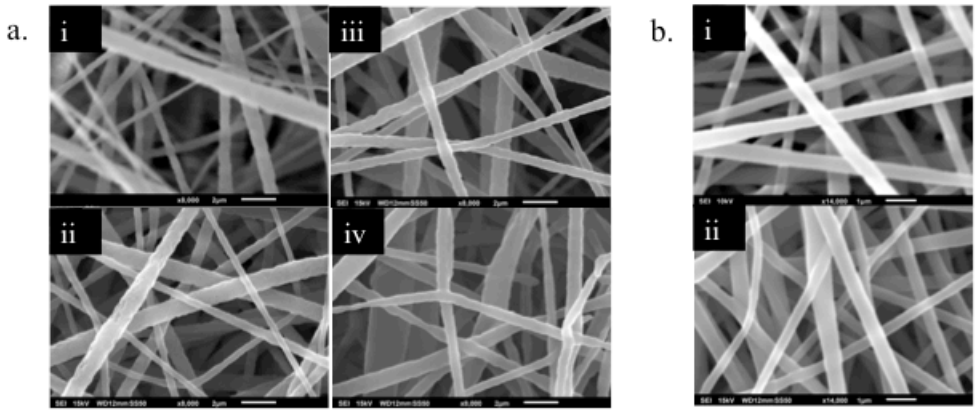

Figure 2. SEM images of PSU mats with average, as-spun fiber diameters of (a.) 0.8μm and (b.) 0.4μm, annealed at different temperatures. a.i) As-spun PSU with an average fiber diameter of 0.8μm; a.ii) PSU annealed at 190°C with a post-treatment average fiber diameter of 0.8μm; a.iii) PSU annealed at 200°C with a post-treatment average fiber diameter of 0.8μm; a.iv) PSU annealed at 210°C with a post-treatment average fiber diameter of 0.9μm. b.i) As-spun PSU with an average fiber diameter of 0.4μm; b.ii) PSU annealed at 210°C with a post-treatment average fiber diameter of 0.4μm. The scale bars are 2μm and 1μm for the micrographs in (a.) and (b.), respectively.

Table1: Compressibility properties of wet electrospun mats and the *kE* value obtained from the line of best fit for permeance curves. The error bars reported were obtained from the standard deviation of five replicates. The standard deviations of the *kE* values are comparable to the orders of magnitude; these values should be interpreted with caution.

Fiber diameter (μm)	Annealing temperature (°C)	Initial solidity, ϕ_0	*n* value	(*kE*) value measured mechanically (kPa)	Best fit *kE* value from permeation (kPa)
0.4 ± 0.1	210	0.07 ± 0.01	7.4 ± 0.3	(3.3 ± 2.8) x 10^4	3.7 x 10^6
0.8 ± 0.4	190	0.10 ± 0.02	6.4 ± 0.3	(5.7 ± 1.8) x 10^5	8.5 x 10^4
0.8 ± 0.3	200	0.10 ± 0.02	7.67 ± 0.08	(8.0 ± 1.4) x 10^5	7.3 x 10^5
0.9 ± 0.4	210	0.09 ± 0.01	8.3 ± 0.3	(2.7 ± 1.5) x 10^6	1.2 x 10^6

4.2 Compression. Mechanical compression tests were performed on the annealed electrospun mats in the wet condition to obtain the compressibility parameters *n* and *kE* from Toll's model. The values of these two parameters increase with increasing

annealing temperature, as reported in Table 1. This trend was also observed in compression tests performed on dry electrospun mats [22] but *n* values for the electrospun mats are consistently higher when fully wetted.

4.3 Permeance. Figure 3a shows that permeance decreases with an increase in pressure drop for all of the electrospun PSU fiber mats. This is compelling evidence that the solidities of the electrospun mats increase as a result of compression under pressure driven flow. The permeance of the PSU mat with smaller fiber diameter is smaller than that of the PSU mats with bigger fiber diameter over the range of pressure drops tested. This is in agreement with the fiber diameter dependence of Happel's permeability model, and is due to the higher specific area of contact between fiber and fluid that is associated with smaller diameter fibers.

Ideally, it should be possible to predict the permeance of an electrospun mat using Toll's compressibility equation with *n* and *kE* measured independently by the compression test; however, as previously reported [22], there is a large uncertainty in the values of kE obtained experimentally, due to inhomogeneities both in the original mat and as well as variations in the response of each replicate to mechanical conditioning. Therefore, the *kE* value was treated here as the single adjustable parameter. By fitting the *kE* value, the permeation model was able to predict the permeance in good agreement with the experimental permeance of all four sets of PSU mats ($R^2 > 0.94$). The values of *kE* obtained by permeance testing for all PSU mats are similar to those obtained by compression testing, except for the PSU mats with 0.4μm fiber diameter, for which the value obtained by permeation is two orders of magnitude higher than the value obtained by compression. The *kE* values are tabulated in Table 1.

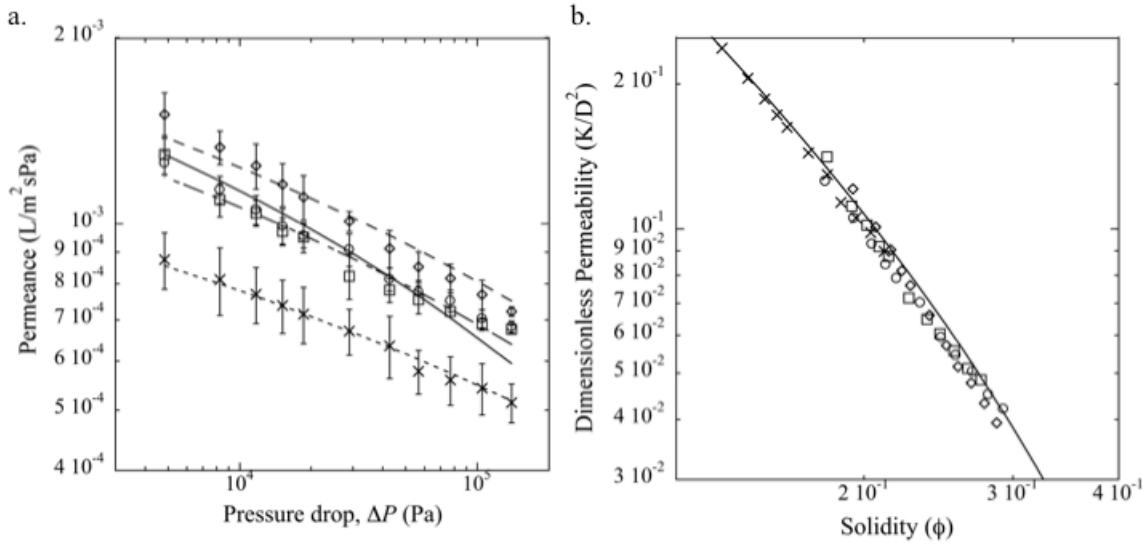

Figure 3. a) Experimentally measured permeances (symbols) and best fits of model (i.e. minimal sum of least squares residuals, lines) plotted against pressure drop for the PSU mats with 0.8μm fiber diameter annealed at 190°C (circles, solid line), PSU with 0.8μm fiber diameter annealed at 200°C (squares, dot-dashed line), PSU with 0.9μm fiber diameter annealed at 210°C (diamonds, dashed line), and PSU with 0.4μm fiber diameter annealed at 210°C (crosses, dotted line); the values of n and kE used in the model are reported in Table 1. b) The permeance from a) converted to dimensionless permeability K/D^2 vs. solidity and compared with Happel's equation for the dimensionless permeability K/D^2 (from Eq. 4). The symbols in (b) are the same as for (a); the solid line is Happel's model.

The data for permeance vs. pressure drop can be converted to a dimensionless permeability (K/D^2) using Eq 4 and the overall compression (or average solidity) of the mat predicted by the model:

$$\frac{K}{D^2} = \frac{J\mu\Delta z}{\Delta P D^2} \tag{9}$$

where Δz is the thickness of the electrospun mat estimated from the permeation model with the optimized kE value. The mat thickness was also used to calculate the average solidity of the mats at each pressure drop.

$$\phi = \frac{m/\rho}{A_{perm}\Delta z} \tag{10}$$

where m is the mass of the electrospun mat; ρ is the density of bulk PSU; and A_{perm} is the area of the electrospun mat used for the permeation test.

According to Happel, K/D^2 should be a function of solidity only. The data for the four mats collapse into a single curve, after the effects of fiber diameter and compression of the mats are taken into account, as shown in Figure 3b. This confirms that Happel's model describes the experimental permeability well. Perhaps more importantly, it also confirms that the compression predicted by the model using Toll's equation accurately describes the change in solidity with applied hydraulic pressure.

Figure 4 shows the profiles for hydraulic pressure (as a fraction of total pressure) and solidity through the thickness of the PSU mat with a fiber diameter of 0.9μm, annealed at 210°C. As seen from the same figure, the largest increase in solidity occurs near the upstream of the membrane (near z = 0). This is because the sample has a high n value (n=8.3); hence the term $d\phi/d\sigma_m$ is large at small solidity, according to Eq. 6. However, the high n value ultimately results a decrease in $d\phi/d\sigma_m$ as the solidity increases.

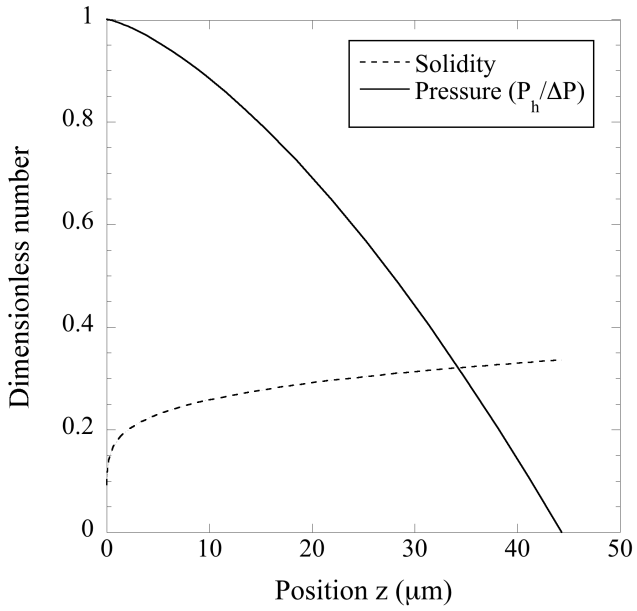

Figure 4. Pressure (solid line) and solidity (dotted line) profile along the z-axis of an electrospun PSU mat annealed at 210C, having an initial solidity of 0.09 and initial thickness of 136μm. The pressure drop applied here was 140 kPa.

For purposes of comparison, permeation and compression tests were also performed on a commercial microfiltration membrane, MF, with a nominal pore size of 3μm. The MF membrane is not fibrous in structure, and is made using a different process. Figure 5a

shows the measured permeability constant for the MF membrane compared to those of the electrospun membranes. The permeability constant of the MF membrane was calculated by assuming that the membrane was incompressible, with thickness of 167 ± 2μm. The solidity increased only by ~0.01 when a pressure of 64 kPa was applied during the compression test, as shown in Figure 5b. The permeability of the MF membrane is higher than those of the PSU mats over the range of pressure from 5kPa to 140 kPa tested in this work, even though the initial solidity of the electrospun mats is lower. This suggests that the electrospun mats may perform better at pressures below about 1 kPa, but perform less well at higher pressures due to the increase of solidity that comes with the higher compressibility of the PSU mats. The solidity of the PSU mats becomes higher than that of MF membrane at ~1 kPa, as seen in Figure 5b.

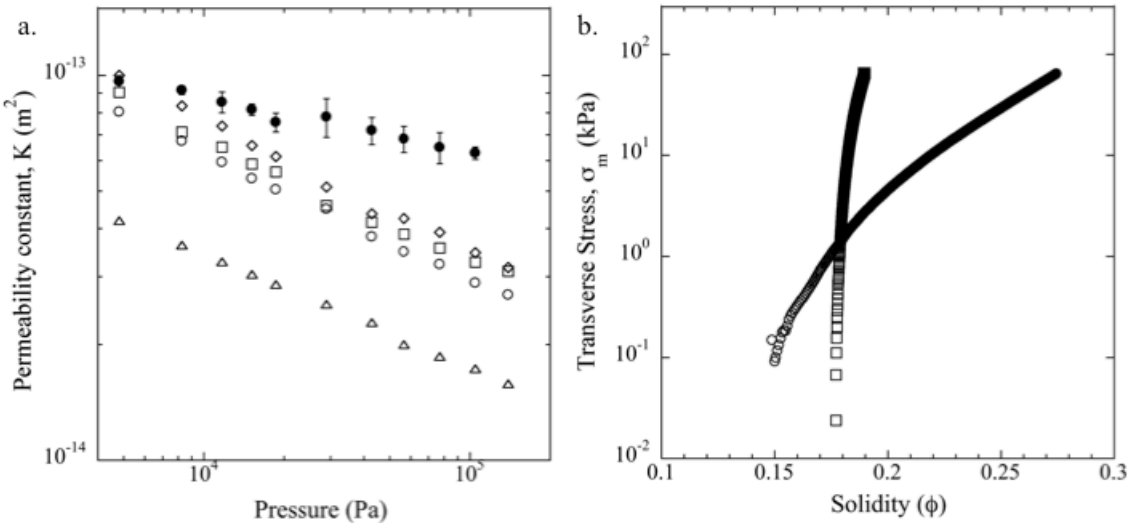

Figure 5 a) Experimental permeability constant (Eq. 9) vs. pressure drop for PSU with 0.8μm fiber diameter annealed at 190°C (circles), PSU with 0.8μm fiber diameter annealed at 200°C (squares), PSU with 0.9μm fiber diameter annealed at 210°C (diamonds), PSU with 0.4μm fiber diameter annealed at 210°C (triangles), and microfiltration membrane with 3μm pore size (filled circles); b) the stress vs. solidity plot for microfiltration membrane with 3μm pore size (squares) and PSU with 0.9μm fiber diameter annealed at 210°C (circles).

5. Conclusions

The permeabilities of electrospun mats under pressure driven flow are shown to be well described by a model for compressible fibrous media that uses Darcy's law for pressure-driven flow with Happel's model for permeability and Toll's model for compressibility.

The solidity increases along the z-axis in the flow direction, and the rate of increase of the solidity depends on the compressibility (parameterized by *n* and *kE*) of electrospun mats. The permeability test provides an alternative method to estimate the kE values of electrospun mats in addition to direct measurement via compression tests. Due to their compressive nature, electrospun PSU mats perform well at low pressure (P < 1kPa), but this advantage of high porosity is soon lost with increasing pressure..

Acknowledgement

The authors would like to thank Matthew Mannarino and Philip Reiser for the useful discussions and support with the permeation experiments. The funding of this project was provided by King Fahd University of Petroleum and Minerals (KFUPM) in Dhahran, Saudi Arabia, through the Center for Clean Water and Clean Energy at MIT and KFUPM under PROJECT NUMBER R5-CW-08. We would also like to acknowledge the Institute for Soldier Nanotechnology at MIT for use of facilities.

References

[1] K. Yoon, B. Hsiao, B. Chu, *J. Mater. Chem.* **18** (2008) 5326-5334.
[2] C. Burger, B. Hsiao, B. Chu, *Annu Rev Mater Res* **36** (2006) 333-368.
[3] N. Li, A. Fane, W. Ho, T. Matsuura, *Advanced Membrane Technology and Applications*, Wiley, New Jersey, 2008, pp.102, Fig.5.1.
[4] M.A. Biot, *J. Appl. Phys.* **12** (1941) 426-430.
[5] M.A. Biot, *J. Appl. Phys*. **26** (1955) 182-185.
[6] W.M. Lai, Van C. Mow, V. Roth, *Journal of Biomechanical Engineering,* **103** (1981) 61-66.
[7] Van C. Mow, M. H. Holmes, W. M. Lai, *J. Biomechanics*, **17** (1984) (5) 377-394.
[8] S. Zhu, R.H. Pelton, K. Colliver, *Chemical Engineering Science*, **50** (1995) (22) 3557-3572.
[9] M. Kataja, K. Hiltunen, J. Timonen, *J. Phys. D: Appl. Phys.* **25** (1992) 1053-1063.
[10] K.A. Jönsson, B.T.L. Jönsson, *AIChE Journal.* **38** (1992) (9) 1340-1348.
[11] K.A. Jönsson, B.T.L. Jönsson, *AIChE Journal.* **38** (1992) (9) 1349-1356.
[12] J. Happel,*AIChE. J*. **5** (1959) 174-177.
[13] J.E. Drummond, M.I. Tahir, *Int. J. Multiphase Flow* **10** (1984) 515-540.
[14] S. Kuwabara, *J. Phys. Soc.* **14** (1959) 527-532.
[15] L. Spielman, S.L. Goren, *Envir. Sci. and Tech.* **2** (1968) 279-287.
[16] N. Mao, S.J. Russell, *J. Text. Inst.* **91** (2000) (2) 235-243.
[17] N. Mao, S.J. Russell, *Text. Res. J.* **73** (2003) (11) 939-944.
[18] C.N. Davies, *Air Filtration,* Academic, London, 1973.
[19] D.S. Clague, R.J. Phillips, *Phys. Fluids* **9** (1997) (6) 1562-1572.

[20] T.J. Donohue, C.M. Wensrich, *Powder Technology* **195** (2009) 57-62.
[21] G.W. Jackson, D.F. James, *The Canadian Journal of Chemical Engineering* **64** (1986) 364-374.
[22] L.T. Choong, M.M. Mannarino, S. Basu, G.C. Rutledge , *J. Memb. Sci.* (in press) (2013)
[23] S. Toll, *Polymer Engineering & Science* **38** (1998) (8) 1337-1350.
[24] M.M. Mannarino, G.C. Rutledge, *Polymer* **56** (2012) 3017-3025.
[25] ASTM Standard D575, 1991 (2012), Standard Test Methods for Rubber Properties in Compression, *ASTM International*, West Conshohocken, PA, 2012.